Schwann cell precursors contribute to skeletal formation during embryonic development in mice and zebrafish

Meng Xie (谢梦)[a], Dmitrii Kamenev[b], Marketa Kaucka[a,c], Maria Eleni Kastriti[a,c], Baoyi Zhou[a], Artem V. Artemov[c,d], Mekayla Storer[e], Kaj Fried[b], Igor Adameyko[a,c], Vyacheslav Dyachuk[b,f,1], and Andrei S. Chagin[a,d,1]

[a]Department of Physiology and Pharmacology, Karolinska Institutet, 17165 Solna, Sweden; [b]Department of Neuroscience, C4, Karolinska Institutet, 17165 Solna, Sweden; [c]Department of Molecular Neurosciences, Medical University of Vienna, A-1090 Vienna, Austria; [d]Institute for Regenerative Medicine, Sechenov University, 119992 Moscow, Russia; [e]Program in Neurosciences and Mental Health, Hospital for Sick Children, Toronto, ON M5G IL7, Canada; and [f]National Scientific Center of Marine Biology, Far Eastern Branch, Russian Academy of Sciences, 690041 Vladivostok, Russia

Immature multipotent embryonic peripheral glial cells, the Schwann cell precursors (SCPs), differentiate into melanocytes, parasympathetic neurons, chromaffin cells, and dental mesenchymal populations. Here, genetic lineage tracing revealed that, during murine embryonic development, some SCPs detach from nerve fibers to become mesenchymal cells, which differentiate further into chondrocytes and mature osteocytes. This occurred only during embryonic development, producing numerous craniofacial and trunk skeletal elements, without contributing to development of the appendicular skeleton. Formation of chondrocytes from SCPs also occurred in zebrafish, indicating evolutionary conservation. Our findings reveal multipotency of SCPs, providing a developmental link between the nervous system and skeleton.

Schwann cell precursors | mesenchymal cells | cartilage | bone | glia

Cartilage is elastic tissue containing specialized chondrocytes, promoting endochondral bone growth and facilitating articulation of skeletal elements. Bone is constantly remodeled: Osteoblasts secrete the matrix required; osteocytes generated from osteoblasts modulate turnover; and osteoclasts resorb the bone. During embryonic development, bones form via either endochondral ossification, where long bones form on a cartilage template, or intramembranous ossification, where flat bones, including the skull and certain craniofacial bones, form by direct differentiation of mesenchymal cells into osteoblasts, with no cartilaginous intermediate.

Chondrocytes and bone-forming cells originate from 3 embryonic lineages: neural crest cells (NCCs) produce facial skeleton (1); paraxial mesodermal cells contribute to cranial and axial skeleton (2); and lateral plate mesodermal cells generate the skeleton of arms and legs (3). At designated locations, these cells form mesenchymal condensations that differentiate into chondrocytes (endochondral ossification) or differentiate into osteoblasts (intramembranous ossification) (4). Formation of transient, multipotent, embryonic NCCs in specific domains of the neuroectoderm during neurulation involves interactions between the neural plate and epidermal ectoderm (5). Thereafter, these cells undergo epithelial-to-mesenchymal transition, delaminate, migrate to the head and trunk, and differentiate into numerous cell types (6). In the head, they become neurons and glia, as well as ectomesenchymal tissues such as cartilage, bone, and other connective tissues of the craniofacial prominence and pharyngeal arches (5).

Schwann cell precursors (SCPs), direct descendants of NCCs, provide trophic and functional support for sensory and motor neurons and their axons (7, 8). SCPs navigate along peripheral axons to various sites, detach, and generate several cell types, including pigment cells (9), parasympathetic and enteric neurons (10, 11), dental mesenchymal cells (12), endoneurial fibroblasts (13), neuroendocrine chromaffin cells of the adrenal medulla (14), and Zuckerkandl organ (15). Thus, SCPs are multipotent, providing cells for various tissues and organs during development,

when NCCs are no longer available (16). However, the role of SCPs in forming skeletal elements remains unknown.

Here, we demonstrate that, during murine embryonic development, SCPs leave peripheral nerves to contribute a few, but significant number of cells to cartilage and bone, both in the craniofacial region and trunk, including the scapula and ribs. A similar phenomenon occurs during zebrafish development.

Results

Specific Genetic Labeling of Embryonic SCPs in the Plp1^{CreERT2} Mouse Line. Proteolipid protein-1 (PLP1), the major myelin protein, is expressed initially by NCCs (17, 18). However, after NCCs have delaminated and migrated [embryonic day 9.5 (E9.5) for the cranium and E10.5 for the trunk (17, 19)], this protein is expressed predominantly by SCPs (9). Accordingly, the SCP lineage can be traced genetically in Plp1^{CreERT2} mice (10–12, 14). To determine whether SCPs contribute to the formation of cartilage and bones, tamoxifen-inducible Plp1^{CreERT2} mice were crossed with a R26R^{YFP} reporter or R26R^{Confetti} multicolor reporter strain (20) by inducing Cre-dependent genetic recombination at either E11.5 or E12.5, when SCPs could be labeled without labeling NCCs (9–12, 14).

The glial specificity of Plp1^{CreERT2} mice was confirmed utilizing SOX10 as a panglial marker (21) and neuron-specific class III β-tubulin (TUJ1) to visualize peripheral nerves (22). The YFP signal visualized with anti-GFP antibodies and immunolabeling of SOX10 were both localized along TUJ1$^+$ nerves in the face and trunk upon short-term tracing from E11.5 to E12.5 (SI Appendix, Fig. S1 A and B), as confirmed by scanning the entire mouse embryo (Movie S1; neurofilaments visualized with 2H3 antibody). Covisualization of Cre protein and GFP signal revealed

Significance

Multipotent Schwann cell precursors (SCPs) generate numerous cell types. Here, in both mouse and zebrafish, SCPs contributed to the generation of mesenchymal, chondroprogenitor, and osteoprogenitor cells during embryonic development. These findings reveal a source of cartilage and bone cells and previously unanticipated interactions between the nervous system and skeleton during development.

recombination efficiencies of 57.8 ± 14.5% (211 GFP$^+$Cre$^+$ per 378 total Cre$^+$ cells) when $Plp1Cre^{ERT2}$:$R26R^{YFP/+}$ mice were traced from E12.5 to E13.5 and 51.22 ± 5.5% (102 double-positive per 199 Cre$^+$ cells) when traced from E15.5 to E16.5 (*SI Appendix*, Fig. S1 *C* and *D*). Similar experiments, employing $Plp1^{CreERT2}$ crossed with $R26R^{Confetti/Confetti}$ mice, confirmed overlap between Cre and Sox10 expression along Tuj1$^+$ nerves (*SI Appendix*, Fig. S1*E*), as well as between Sox10 and Confetti proteins, the latter visualized with anti-GFP antibody, which does not recognize RFP among 4 different confetti proteins, when traced from E12.5 to E13.5 (*SI Appendix*, Fig. S1*F*).

To prove that $Plp1^{CreERT2}$-labeled cells generate Schwann cells, we combined immunodetection of Protein Zero (P0, a Schwann cell marker) with YFP signal retrieval by anti-GFP antibody in $Plp1Cre^{ERT2}$:$R26R^{YFP/+}$ mice traced from E11.5 to either E12.5 or E17.5. The percentage of P0$^+$ among GFP$^+$ cells associated with TUJ1$^+$ nerves rose from 12.3 ± 8% at E12.5 to 56.6 ± 18.6% at E17.5 (*SI Appendix*, Fig. S2 *A–D*), indicating that Schwann cells arose from SCPs.

Arising of murine sympathetic chain ganglia entirely from NCCs (23, 24) allowed confirmation that the latter were not traced. Predictably, neurons (staining for tyrosine hydroxylase [TH]) in sympathetic ganglia were not genetically labeled in $Plp1^{CreERT2}$:$R26R^{YFP}$ embryos upon tracing from either E11.5 or E12.5 to E17.5 (*SI Appendix*, Fig. S2 *E* and *F*). All sympathetic ganglia were scanned for the YFP signal in TH$^+$ sympathetic neurons to exclude leakage of $Plp1^{CreERT2}$ into NCCs.

Altogether, when recombination is induced at E11.5 or E12.5 in $Plp1^{CreERT2}$ mice, SCPs, but not NCCs are genetically labeled, as reported previously (10, 12, 14). Since 12.33 ± 8% of YFP$^+$ cells express a marker for mature Schwann cells after 24-h tracing, some more mature Schwann cells may also be labeled, although these cells can be generated from SCPs during this period.

Spontaneous recombination without tamoxifen was excluded by scanning 7 whole $Plp1^{CreERT2}$:$R26R^{YFP}$ embryos at E11.5 (representative scanning of Cre$^+$ embryo in *SI Appendix*, Fig. S2*G* and Movie S2; 6.5% maximal laser power in Movie S1 versus 50% for Movie S2, which produces autofluorescent signals from internal organs and blood vessels). Furthermore, when the heads of 11 Cre$^+$ $Plp1^{CreERT2}$:$R26R^{YFP}$ embryos from 3 independent litters, either uninjected or injected with corn oil only, were scanned at E17.5, no spontaneous recombination was detected (representative sagittal facial sections in *SI Appendix*, Fig. S2 *H* and *I*). Since more spontaneous recombination is possible with 2 reporter copies, we tested $Plp1^{CreERT2}$ coupled with either 1 or 2 copies of the $R26R^{YFP}$ allele (heterozygotes or homozygotes). Although no recombination occurred without tamoxifen, we minimized the risk of accidental recombination before tamoxifen by performing all subsequent experiments with $R26R^{YFP}$ heterozygous mice (unless otherwise specified). Two copies of the $R26R^{Confetti}$ allele were used to generate more color recombination options.

SCPs Give Rise to Mesenchymal Cells. Since cells of the chondrocyte and osteoblast lineages arise from mesenchymal cells (25), we examined the potential SCP contribution to mesenchymal cells with color-coded genetic tracing of $Plp1^{CreERT2}$:$R26R^{Confetti/Confetti}$ mice from E12.5 to E17.5. Clonal appearance was based on confetti color (Fig. 1*A*), and association with nerves revealed by staining neurons and confetti clones in the same area with the PGP9.5 marker and an anti-GFP antibody, respectively (Fig. 1*B*). At E17.5, some descendants of SCPs initially labeled remained on the nerve, maturing into Schwann cells (arrowheads in *A'*, *A''*, *B'*, and *B''* in Fig. 1 *A* and *B*). Other progenies of the same color, most likely derived from the same progenitors, had detached from the nerves and exhibited typical mesenchymal cell morphology (arrows in *A'*, *A''*, *B'*, and *B''* in Fig. 1 *A* and *B*). These cells formed small, tightly packed clonal patches, distinct from the large clones observed previously with NCC tracing in this $Plp1^{CreERT2}$:$R26R^{Confetti/Confetti}$ strain (26). Note that the orange clone in *A'* arises from the YFP and RFP signals combined, an

occurrence so rare that the likelihood that these cells in such proximity are from different clones is essentially zero (see *SI Appendix* for statistical analysis). At E17.5, 4.6% of the genetically labeled cells with mesenchymal morphology were not associated with nerves (Fig. 1*B*). Immunostaining for PDGFRa, a marker for mesenchymal cells and endoneurial fibroblasts (27), in $Plp1^{CreERT2}$:$R26R^{Confetti/Confetti}$ mice traced from E12.5 to E17.5 revealed that traced cells with mesenchymal appearance stain positively (Fig. 1*C*), confirming their mesenchymal nature.

To exclude direct induction of recombination in mesenchymal cells by $Plp1^{CreERT2}$, we analyzed $Plp1^{CreERT2}$:$R26R^{Confetti/Confetti}$ mice traced from E12.5 to E13.5. Of 1,279 Cre$^+$ cells, only 14 cells expressed PDGFRa and were located outside TUJ1$^+$ nerves (1.09%; 11 embryos quantified). Similarly, of 1,391 GFP$^+$ cells, only 19 were positive for PDGFRa and located outside TUJ1$^+$ nerves (1.37%, 11 embryos analyzed; *SI Appendix*, Fig. S1 *G* and *H*). However, no Cre$^+$YFP$^+$ cells were detected outside TUJ1$^+$ nerves (18 Cre$^+$ or YFP$^+$ cells in 11 embryos), suggesting that 1.09% of Cre$^+$ cells outside nerves do not cause recombination and probably reflect variation due to antibody unspecificity or sporadic Cre too low to induce recombination.

Since nerve-associated PDGFRa$^+$ endoneurial fibroblasts generate mesenchymal cell types during digit regeneration (27), we showed that 2.8% of Cre$^+$ cells along TUJ1$^+$ nerves also express PDGFRa$^+$ (35 of 1,265; *SI Appendix*, Fig. S1*G*). Staining of recombined cells with anti-GFP antibody gave similar results (3.4%; 46 GFP$^+$PDGFRa$^+$ among 1,371 GFP$^+$ cells; *SI Appendix*, Fig. S1*H*), suggesting that recombined cells include only 2.8 to 3.4% potential endoneurial fibroblasts.
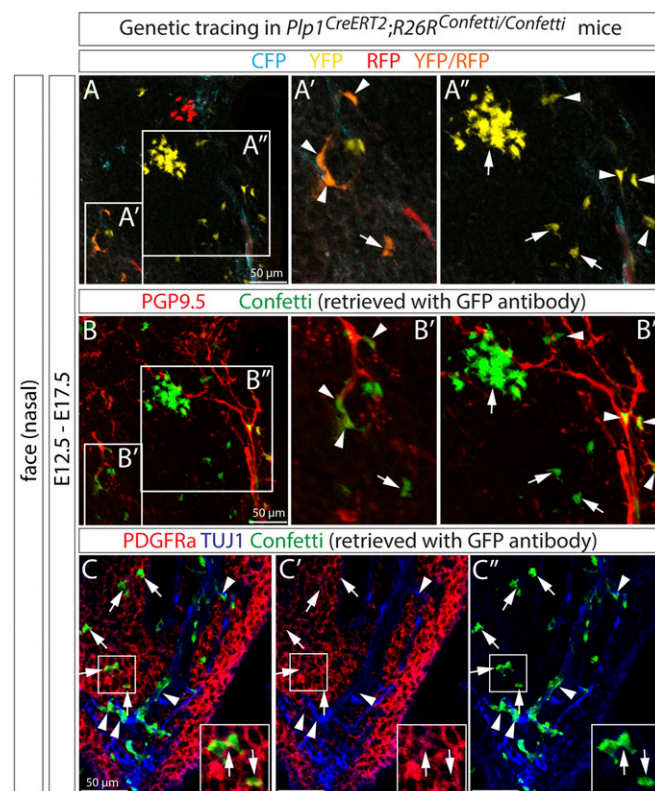
Fig. 1. SCPs generate mesenchymal cells during murine embryonic development. (*A–C*) Genetic tracing of $Plp1^{CreERT2}$:$R26R^{Confetti/Confetti}$ embryos revealed SCP contribution to proximal mesenchymal cells. Confetti clones expressing RFP, YFP, and/or CFP proteins are shown in *A*. The same tissue section was immunostained with PGP9.5 (for neuron) and GFP (for confetti) in *B*. (*C*) The traced cells off TUJ1$^+$ nerves were positive for mesenchymal marker, PDGFRa. In *A–C*, arrowheads indicate traced cells on nerves and arrows indicate traced cells that become mesenchymal cells.

SCPs Contribute to Chondrogenesis. Chondrogenic mesenchymal condensations appear in the murine craniofacial compartment at E12.5, enlarge at E13.5, and become cartilage at E14.5 (28). At E12.5 these condensations express SOX9 (Fig. 2 *A* and *B* and *SI Appendix*, Fig. S3), a marker for both chondroprogenitors and mature chondrocytes (29, 30). Tracing *Plp1^CreERT2^;R26R^YFP/+^* mice from E11.5 to E12.5 revealed virtually no overlap between YFP^+ cells and SOX9^+ chondroprogenitors (4 double-positive among 16,776 SOX9^+ cells in the craniofacial region; none among 6,929 SOX9^+ cells in the ribs and scapula) (Fig. 2 *A* and *B* and *SI Appendix*, Fig. S3*A*). At E12.5 in wild-type nontraced mice as well, no cells expressed both SOX9 and the SCP marker, SOX10 (*SI Appendix*, Fig. S3 *B* and *C*).

At E15.5, TUJ1^+ nerves and associated YFP^+ glial cells (labeled with tamoxifen at E11.5) grew close to cartilaginous elements (orange arrowheads in Fig. 2 *C′* and *D′*, and *C* and *D*). YFP^+ cells dissociated from nerves and some YFP^+SOX9^+ chondrocytes (white arrows and arrowheads, respectively, in Fig. 2 *C′* and *D′*, and *C* and *D*) were also observed. At E17.5, these double-positive cells had separated completely from the neurites, constituting various parts of the facial and trunk skeletons (Fig. 2 *E* and *F* and *SI Appendix*, Fig. S4 *A–G* and *V*). Some YFP^+ cells generated perichondrium cells (orange arrows in Fig. 2 *E′* and *F* and *SI Appendix*, Fig. S4 *A–C*). In craniofacial cartilage, perichondrial cells differentiate into chondrocytes arranged in characteristic transversal columns (28), as occasionally observed here when tracing SCP cells (white arrowheads in *SI Appendix*, Fig. S4 *B* and *C*). In the trunk, SCPs contributed to formation of chondrocytes in the rib and scapula (*SI Appendix*, Fig. S4 *F, G, M, N,* and *V*). Interestingly, these rib chondrocytes originate from the mesoderm (2), suggesting that, by migrating along nerves, SCPs might help form structures other than neural crest derivatives.

Differentiation of SCPs into mature chondrocytes (directly or via mesenchymal or perichondrial intermediate) was confirmed by visualizing YFP^+ cells in regions expressing type II collagen (*SI Appendix*, Fig. S4*X*). Genetic tracing from E12.5, as from E11.5, revealed SCP contribution to various cartilage elements (*SI Appendix*, Fig. S4 *H–N* and *V*), in contrast to tracing from E15.5 (*SI Appendix*, Fig. S4 *O–U* and *V*), suggesting that SCPs differentiate into cartilage transiently, similar to their formation of parasympathetic nerves (10). No contribution to long bone cartilage was observed (*SI Appendix*, Fig. S4*W*). To estimate the SCP contribution, we examined embryos carrying 1 (*R26R^YFP/+^*) or 2 copies (*R26R^YFP/YFP^*) of the YFP reporter, where the frequency of recombination might differ. YFP^+ cells generate up to 10% of the SOX9^+ chondrocytes in homozygous embryos (*SI Appendix*, Fig. S4 *Y* and *Z*). In light of 58% efficiency of Cre recombinase (see above), SCPs might contribute ≥10% of all chondrocytes, rendering this chondrogenesis of considerable biological significance.

SOX10 is a marker of SCPs. We employed *Sox10^CreERT2^* crossed with *R26R^Confetti/Confetti^* mice to further verify the SCP contribution to chondrocytes. Short-term tracing before cartilage is induced (E10.5 to E11.5) showed recombination in SOX10^+ cells along nerves, with no recombination in the SOX9^+ chondrogenic domain (*SI Appendix*, Fig. S5 *A–D*). In total, 1.47% of cells in the SOX9^+ domain of the craniofacial region were GFP^+ (57 of 3,878) and 0.23% in the trunk were (22 of 9,430), whereas 99% of recombined cells were associated with TUJ1^+ nerves, indicating their glial origin. Prolonged tracing (E10.5 to E17.5) revealed contribution to cartilage in both facial and trunk regions (*SI Appendix*, Fig. S5 *E–J*), similar to *Plp1^CreERT2^* genetic tracing. Clearly, Sox10 tracing must be interpreted carefully, since at E9.5 Sox10 labels late NCCs in the craniofacial region, whereas at E12.5 early chondroprogenitors are labeled (26, 28), leaving a narrow time window for specific SCP labeling.

To understand whether the fate of specific SCP populations is restricted, we utilized the *Dhh^Cre^* line. DHH is first expressed by SCPs around E12.0 in a patchy manner (13), suggesting that the DHH^+ subpopulation matures only into Schwann cells and endoneurial fibroblasts (13, 31). Support is provided by only partial
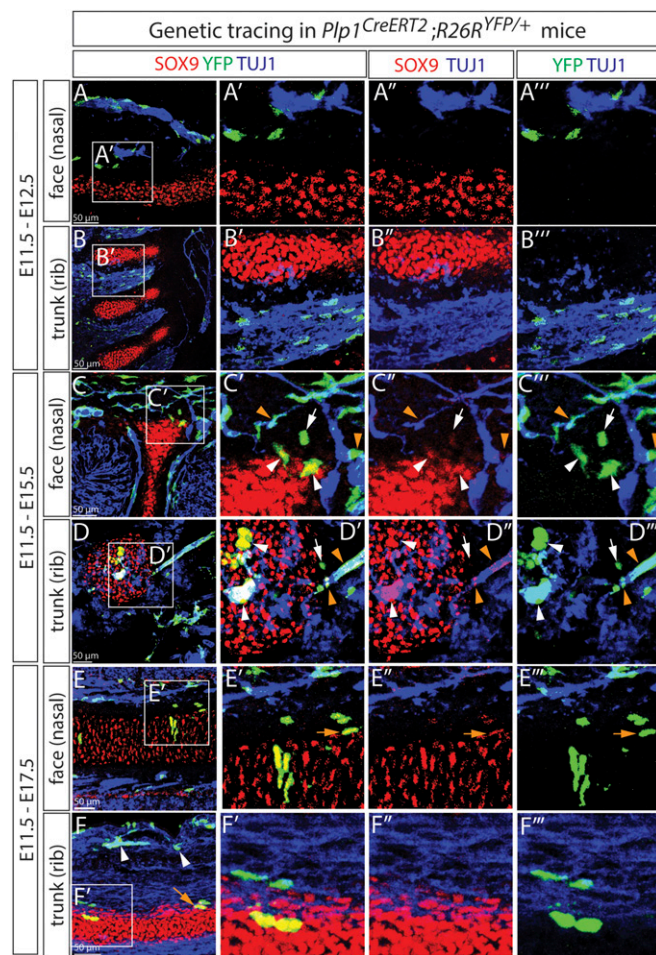
Fig. 2. SCPs generate chondroprogenitors in craniofacial region and trunk during murine embryonic development. Genetic labeling in *Plp1^CreERT2^;R26R^YFP/+^* embryos from E11.5 to E12.5 revealed no overlap between SCPs and SOX9^+ chondroprogenitors (*A* and *B*). Prolonged tracing revealed appearance of SCP progeny in cartilage at E15.5 (*C* and *D*) and E17.5 (*E* and *F*). Orange arrowheads and white arrows indicate YFP^+ cells on TUJ1^+ nerves and close to nerves and cartilage, respectively, and white arrowheads indicate YFP^+SOX9^+ chondrocytes in *C′* and *D′*. The orange arrow in *E′* indicates an YFP^+ perichondrial cell. These images represent at least 5 Cre^+ embryos from independent litters. A total of 5 facial and 2 trunk skeletal elements in each embryo were checked (see *SI Appendix*, Fig. S4 for details).

overlap between SOX10^+ and DHH^+ populations along TUJ1^+ neurites at E12.5 (11.6%; range, 2.2 to 21.9%) Tomato^+SOX10^+ cells within the SOX10^+ population in the face and 6.9% (2.0 to 17.8%) in the trunk (*SI Appendix*, Fig. S6 *A* and *B*). In addition, DHH^+ cells did not contribute to the sympathoadrenal anlage (marked with TH antibody), which is formed by SCPs (14) (*SI Appendix*, Fig. S6*C*). As expected, Dhh^+ SCPs did not contribute to cartilage and instead generated scattered Schwann cells within nerve bundles at E17.5 (*SI Appendix*, Fig. S6 *D–H*). This suggests that SCPs becomes heterogeneous around E12.5, and not all late subpopulations give rise to mesenchymal tissue, including cartilage.

Altogether, these observations provide proof-of-principle that embryonic SCPs contribute to formation of various cartilage elements of the skeleton.

SCPs Contribute to Osteogenesis. Next, we examined potential contribution of peripheral glial cells to formation of the osteoblast lineage, beginning with osteoblast progenitors and utilizing the transcription factors Osterix (OSX) and Runx2 as markers. Genetic tracing of *Plp1^CreERT2^;R26R^YFP/+^* embryos from either E11.5 or

E12.5 to E17.5 revealed colocalization of YFP with either marker in bones (Fig. 3 *A–C* and *SI Appendix*, Fig. S7 *A–C, D, and E*). The greatest contribution to osteoprogenitors, in the mandibular region, was not dramatic ($2.1\pm 0.22\%$; Fig. 3*D*). No YFP$^+$ osteoprogenitors were observed during tracing from E15.5 to E17.5 (Fig. 3*D*). DMP1 and E11, markers for osteocytes (32), showed that some YFP$^+$ cells differentiate into DMP1-expressing osteocytes (Fig. 3 *E* and *F*) in E11$^+$ and DMP1$^+$ bone regions (*SI Appendix*, Fig. S7 *F–I*). Importantly, ossified elements in the craniofacial region appear initially only at E15.5 (28), several days after our genetic labeling.

Altogether, these experiments suggest that during embryonal bone formation an SCP subpopulation contributes to the osteoblast lineage, including preosteoblasts and osteocytes.

The SCPs' Contribution to Skeletogenesis Has Been Conserved Evolutionarily from Zebrafish to Mice. The contribution of glial cells to skeletal development was also explored in *Sox10^{CreERT2};Ubi:zebrabow* zebrafish (33), which express YFP or CFP upon 4-hydroxytamoxifen-induced recombination. Only YFP$^+$ cells could be monitored because of greater signal and imaging constraints.

During development of wild-type AB zebrafish larva from 24 to 48 h postfertilization (hpf), cells stained with anti-SOX10 antibody were associated closely with nerves, i.e., they were SCPs and peripheral glial cells (*SI Appendix*, Fig. S8 *A–D*). Tracing in *Sox10^{CreERT2};Ubi:zebrabow* fish from 24 to 48 hpf revealed overlap between YFP and SOX10 along nerves (*SI Appendix*, Fig. S8 *E* and *F*), indicating that Cre-dependent recombination results in genetic tracing of SCPs. Although cartilage elements in the facial region of zebrafish larvae start to form at about 60 hpf, the area between the otic vesicle and first somite showed traces of alcian blue staining at 48 hpf (*SI Appendix*, Fig. S8*G*), and immunohistochemistry revealed the first SOX9a$^+$ chondroprogenitors around the otic vesicle (*SI Appendix*, Fig. S8*H*). During 24-h tracing (24 to 48 hpf), some SOX10-traced cells detached from the nerves but did not express SOX9a (*SI Appendix*, Fig. S8*I*; 6 double-positive of 395 YFP$^+$ cells). Surprisingly, occasional YFP$^+$ cells located along the nerves expressed SOX9a (*SI Appendix*, Fig. S8*J*).

With recombination at 24 or 48 hpf and tracing until 44 d postfertilization (dpf), late juvenile stage, SCPs contributed to various craniofacial skeletal structures in a spatially compact manner, suggesting clonal origin of labeled chondrocytes and of rare cartilage patches in pharyngeal (ceratohyal), mandible (palatoquadrate), and chondrocranial (parachordal) regions and the ear (otic vesicle) ($5.3 \pm 1.1\%$ and $8.3 \pm 1.5\%$ of the cells present during the 2 tracing periods, respectively) (*SI Appendix*, Fig. S9 *A–H*). As in mice, patches of YFP$^+$ chondrocytes were often located adjacent to flat YFP$^+$ perichondrial cells (orange arrows in *SI Appendix*, Fig. S9 *A, B, D, F, and G*). Visualization of cartilage with SOX9a antibody confirmed the contribution of traced cells to various skeletal elements (*SI Appendix*, Fig. S9 *I–P*). Thereafter, crossing *Sox10^{CreERT2};Ubi:zebrabow* with *Col2-mCherry* zebrafish showed early chondrogenesis simultaneously with tracing of SCPs. Live imaging of these fish when chondrogenesis began and several days later revealed no overlap between YFP$^−$ and mCherry$^+$ cells when Sox10$^+$ cells were traced from 24 to 54 hpf or from 48 to 72 hpf, whereas YFP$^+$ chondrocytes appeared at 120 hpf (*SI Appendix*, Fig. S9 *Q* and *R*). Importantly, chondrocytes in zebrafish express SOX10, a common marker for cartilage. We labeled SCPs before chondrocyte formation, i.e., 24 or 48 hpf (at 48 hpf chondrogenesis starts around the otic vesicle; see above). However, to compare glial contribution to that of genetically labeled chondrocytes, we exposed *Sox10^{CreERT2}; Ubi:zebrabow* fish to 4-hydroxytamoxifen at 5 dpf (when pharyngeal cartilage forms), 7 dpf (this formation is complete), or 11 dpf (metamorphosis), and traced until 44 dpf. Labeling at 5 dpf resulted in large clusters of YFP$^+$ chondrocytes (*SI Appendix*, Fig. S8*K*), with almost all cartilage elements labeled at 7 or 11 dpf (*SI Appendix*, Fig. S8 *L* and *M*). In all cases, the labeling pattern was distinct from that of SCPs, where only small, probably clonal

Fig. 3. SCPs generate osteoprogenitor cells and osteocytes in facial region and trunk during murine embryonic development. (*A–C*) SCPs progeny in *Plp1^{CreERT2};R26R$^{YFP/+}$* embryos traced from E11.5 to E17.5 were positive for osteoprogenitor marker OSX in the ossified parts of mandible (*A*), rib (*B*), and scapula (*C*). The white arrowheads indicate double-positive cells. (*D*) Quantification of YFP$^+$ cells among the OSX$^+$ population. Data represent mean ± SEM where at least 3 embryos from independent litters were analyzed. (*E* and *F*) The same traced embryos were positive for Dmp1 RNA probe. *A''''*, *B''''*, and *C''''* depict the same tissue sections as *A–C* but stained with von Kossa and Alcian blue (vK and Ab). The white dashed lines outline the mineralized portion of the bone.

clusters of several YFP$^+$ chondrocytes were observed (*SI Appendix*, Fig. S9 *A–H*).

Altogether, these experiments suggest that, as in mice, SCPs contribute to skeletogenesis in zebrafish.

Discussion

Novel, fundamentally noncanonical roles of the peripheral nervous system discovered recently include tissue regeneration (34), controlling stem cell niches (35), relaying fine positional information (36), and delivering multipotent cells to various locations (14). In the latter connection, SCPs are emerging as a new class of multipotent progenitor cells active during both embryogenesis and postnatal life (10–12, 14), although their potential remains to be elucidated in detail. Here, genetic tracing demonstrated that a small, but significant fraction of SCPs generate mesenchymal cells and chondroprogenitors and osteoprogenitors, expanding their destinies and emphasizing their multipotency. This capacity was limited to embryonic days E11.5 to E15.5 in the mouse,

a time window similar to SCP-dependent generation of chromaffin cells in the adrenal medulla (14) and parasympathetic neurons (10). This window closes as SCPs commit to their fate, becoming phenotypically intermediate, immature Schwann cells (14).

NCCs are immediate progenitors of craniofacial ectomesenchymal cells, as well as multipotent SCPs (37). We show that SCPs generate craniofacial mesenchymal cells, resembling their differentiation into dental mesenchyme (12). These are strong indications that, after leaving nerves, SCPs retain the capacity of their developmental ancestors to produce various mesenchymal populations. One potential explanation might involve developmental constrains posed by the transience of NCCs. Condensation of cartilaginous mesenchymal (i.e., SOX9$^+$) in murine craniofacial regions begins around E12.5, well after NCC migration (E9.5) (19, 26, 28). Thus, SCPs potentially provide additional plastic, local, targeted source of mesenchymal progenitors during late skeletogenesis. Although in mice SCP contribution to craniofacial development might not be significant, other animals, which develop longer or larger animals, such as humans, might need these additional cells for proper skeletogenic development. This resembles the strategy apparently involved in late generation of chromaffin cells in the adrenal medulla (14) or parasympathetic ganglia (10).

This SCP-derived chondrogenesis might be directly related to the condensing mesenchyme, consisting of SCP progeny. If so, mesenchymal cells derived from SCPs can differentiate into cartilage or bone, depending on location, analogous to the position-based differentiation of mesenchymal cells derived from NCCs in the craniofacial region (26). Alternatively, the perichondrium, a thin layer of mesenchymal-type cells surrounding embryonic cartilage elements, may be an intermediate stage. Although cartilage is not innervated, the surrounding perichondrium becomes highly innervated after formation of the skeletal elements (ref. 38 and own observations), i.e., after E12.5, when NCC migration is complete. Accordingly, SCPs may be delivered to the perichondrium during innervation and generate additional mesenchymal cells that produce clusters of labeled chondrocytes. Indeed, generation of chondrocytes by perichondral cells does occur (28). In support of this intermittent role, we observed no SOX10$^+$ SCPs near SOX9$^+$ chondrogenic condensations at E12.5, whereas SCP contribution to cartilage elements begins when the nerves extend closer to these elements. In many cases, labeled cells remain present in both the perichondrium and underlying chondrocytes. Furthermore, many clones were transversal, strongly resembling formation of craniofacial cartilage from the perichondrium by intercalation (28). This might fine-tune cartilage shape by spatially constraining delivery of progeny cells from the perichondrium (28). However, the relatively few chondrocytes derived from SCPs and the lack of any specific spatial distribution argue against this.

The SCP contribution to the perichondrium is especially pronounced in zebrafish, indicating evolutionary conservation, as with SCP differentiation into melanocytes (16). This ancient SCP multipotency is further demonstrated by their capacity to generate the enteric nervous system in cyclostomes (lamprey) (39). However, the evolutionary origin of this multipotency remains unclear (40). In interpreting our findings with zebrafish, one must remember that Sox10, employed for genetic tracing of SCPs, is also expressed by mature chondrocytes. Although we labeled SCPs before chondrogenesis onset and observed no overlap between Sox10-labeled cells and the early marker of chondroprogenitors Sox9a outside nerves, some labeled mesenchymal cells other than SCPs, may have contributed to skeletal elements.

In bony structures, OSX$^+$ and Runx2$^+$ cells are considered to be osteoprogenitors (41). We found that SCPs generate such cells as well as osteocytes. For endochondral ossification, OSX$^+$ osteoprogenitors from the perichondrium migrate into skeletal elements, which are initially cartilaginous, along with blood vessels (42, 43). Thus, like cartilaginous elements, the initial SCP contribution to the perichondral mesenchyme may be followed by development and migration of OSX$^+$ osteoprogenitors from the perichondrium inside ossified skeletal elements. With

intramembranous ossification, the origin of OSX$^+$ cells is less clear, presumably involving direct differentiation of mesenchymal cells into osteoprogenitors. Our findings suggest that at least some OSX$^+$ osteoprogenitors originate from peripheral glial cells of associated nerves. Although this contribution is limited, $Plp1^{CreERT2}$ recombination is 50 to 60% (ref. 10 and own observations) and the YFP signal was retrieved with an antibody as well, which underestimates the actual SCP contribution to osteogenesis. Thus, although relatively minor, the supply of SCPs to both chondroprogenitors and osteoprogenitors could be at least twice that estimated here.

We observed that SCPs contribute to formation of multiple skeletal parts arising either via intramembranous ossification (mandible, subscapular fossa) or endochondral ossification (rib, acromion, and coracoid processes of the scapula), as well as nasal and otic cartilage. Such contribution of neural crest derivatives to trunk skeletal elements contradicts the classical view, although a mixture of mesodermal and NC derivatives do contribute to the scapula (44). This contribution to the ribs, which originate from paraxial mesoderm (44), excluding any direct NCC contribution, is particularly interesting. This suggests that SCPs migrating along developing nerves generate cells that form skeletal elements largely of nonneural crest origin. The reason for mixing descendants of different developmental origins in the same structures remains unexplained. We observed no SCP contribution to long bones of limbs or paws. Another report suggests that NCCs and their progeny (including SCPs) contribute to stromal cells in the marrow of limb bones late during embryonic development and at early postnatal age (45). That study involved noninducible $Wnt1^{Cre2}$ mice, utilizing the Wnt1 promoter in NCCs, from E8.5 to E9.5. However, several recent reports indicate that this promoter is active in bone cells (46–49), so secondary activation of $Wnt1^{Cre2}$ in those differentiated cells might explain the labeling observed (45). In support of this, we detected no NCC contribution to the limbs upon inducing recombination in these cells by injecting tamoxifen into $Sox10^{CreERT2};R26R^{Confetti}$ mice at E8.5, in line with the classical view concerning tissues to which NCCs contribute (50). As we discussed recently, genetic experiments with noninducible Cre mice must be interpreted carefully, due to potential nonspecific promoter activity during ontogenesis (51).

Various interactions between the nervous system and skeleton have long been proposed (12, 45, 52). We demonstrate that during murine embryogenesis, glial progenitors associated with peripheral nerves differentiate directly (although rarely) into skeletal progenitors. Whether these progenitors retain intimate interactions with the nervous system or differ from other skeletal progenitors remains unknown. At present, it is unclear whether glia contribute to skeletogenesis during the postnatal period. Such contribution was not observed after E15.5 here, but this does not exclude reactivation under pathological conditions or following trauma, e.g., bone fracture. Although we observed no contribution by endoneurial fibroblasts to skeletal cells during embryonic development, this clearly happens during trauma (27). Finally, although less likely, we cannot exclude involvement of mature Schwann cells in skeletogenesis, since 12% of them were labeled during genetic tracing. However, this does not alter our conclusions concerning interplay between the nervous system and developing skeleton, since both SCPs and Schwann cells belong to the peripheral nervous system. In summary, precursors of peripheral glial cells can differentiate into skeletal progenitors during embryonic development. This glial skeletogenesis represents a previously unanticipated interaction between the nervous and skeletal systems.

Materials and Methods

Mice and Zebrafish. All animal work was permitted by the Ethical Committee on Animal Experiments (Stockholm North Committee) and conducted according to The Swedish Animal Agency's Provisions and Guidelines. The $Plp1^{CreERT2}$, $R26R^{YFP}$, $Sox10^{CreERT2}$, $R26R^{Confetti}$, and Dhh^{Cre} mice (18, 20, 27, 53) and $Sox10^{CreERT2}$ (54) and *Ubi:zebrabow* (33) zebrafish have been

described. *Col2:mCherry* zebrafish were a gift from Chrissy Hammond, School of Physiology and Pharmacology, University of Bristol, Bristol, UK (55).

Immunohistochemistry. Immunohistochemistry and whole-mount embryo staining were performed as described (14, 19, 51).

RNAscope. RNAscope was performed according to ACD Bio's manual using the Dmp1 probe (ACD Bio; no. 441171), followed by overnight incubation with primary antibody.

See extended methodological details in *SI Appendix, SI Material*.

1. D. M. Noden, Cell movements and control of patterned tissue assembly during craniofacial development. *J. Craniofac. Genet. Dev. Biol.* **11**, 192–213 (1991).
2. P. P. Tam, P. A. Trainor, Specification and segmentation of the paraxial mesoderm. *Anat. Embryol. (Berl.)* **189**, 275–305 (1994).
3. M. J. Cohn, C. Tickle, Limbs: A model for pattern formation within the vertebrate body plan. *Trends Genet.* **12**, 253–257 (1996).
4. B. K. Hall, T. Miyake, The membranous skeleton: The role of cell condensations in vertebrate skeletogenesis. *Anat. Embryol. (Berl.)* **186**, 107–124 (1992).
5. A. Graham, The neural crest. *Curr. Biol.* **13**, R381–R384 (2003).
6. E. Dupin, S. Creuzet, N. M. Le Douarin, The contribution of the neural crest to the vertebrate body. *Adv. Exp. Med. Biol.* **589**, 96–119 (2006).
7. K. R. Jessen *et al.*, The Schwann cell precursor and its fate: A study of cell death and differentiation during gliogenesis in rat embryonic nerves. *Neuron* **12**, 509–527 (1994).
8. A. N. Garratt, S. Britsch, C. Birchmeier, Neuregulin, a factor with many functions in the life of a Schwann cell. *BioEssays* **22**, 987–996 (2000).
9. I. Adameyko *et al.*, Schwann cell precursors from nerve innervation are a cellular origin of melanocytes in skin. *Cell* **139**, 366–379 (2009).
10. V. Dyachuk *et al.*, Neurodevelopment. Parasympathetic neurons originate from nerve-associated peripheral glial progenitors. *Science* **345**, 82–87 (2014).
11. I. Espinosa-Medina *et al.*, Neurodevelopment. Parasympathetic ganglia derive from Schwann cell precursors. *Science* **345**, 87–90 (2014).
12. N. Kaukua *et al.*, Glial origin of mesenchymal stem cells in a tooth model system. *Nature* **513**, 551–554 (2014).
13. N. M. Joseph *et al.*, Neural crest stem cells undergo multilineage differentiation in developing peripheral nerves to generate endoneurial fibroblasts in addition to Schwann cells. *Development* **131**, 5599–5612 (2004).
14. A. Furlan *et al.*, Multipotent peripheral glial cells generate neuroendocrine cells of the adrenal medulla. *Science* **357**, eaal3753 (2017).
15. M. E. Kastriti *et al.*, Schwann cell precursors generate the majority of chromaffin cells in Zuckerkandl organ and some sympathetic neurons in paraganglia. *Front. Mol. Neurosci.* **12**, 6 (2019).
16. J. Petersen, I. Adameyko, Nerve-associated neural crest: Peripheral glial cells generate multiple fates in the body. *Curr. Opin. Genet. Dev.* **45**, 10–14 (2017).
17. L. Hari *et al.*, Temporal control of neural crest lineage generation by Wnt/β-catenin signaling. *Development* **139**, 2107–2117 (2012).
18. D. P. Leone *et al.*, Tamoxifen-inducible glia-specific Cre mice for somatic mutagenesis in oligodendrocytes and Schwann cells. *Mol. Cell. Neurosci.* **22**, 430–440 (2003).
19. I. Adameyko *et al.*, Sox2 and Mitf cross-regulatory interactions consolidate progenitor and melanocyte lineages in the cranial neural crest. *Development* **139**, 397–410 (2012).
20. H. J. Snippert *et al.*, Intestinal crypt homeostasis results from neutral competition between symmetrically dividing Lgr5 stem cells. *Cell* **143**, 134–144 (2010).
21. K. Kuhlbrodt, B. Herbarth, E. Sock, I. Hermans-Borgmeyer, M. Wegner, Sox10, a novel transcriptional modulator in glial cells. *J. Neurosci.* **18**, 237–250 (1998).
22. M. K. Lee, J. B. Tuttle, L. I. Rebhun, D. W. Cleveland, A. Frankfurter, The expression and posttranslational modification of a neuron-specific beta-tubulin isotype during chick embryogenesis. *Cell Motil. Cytoskeleton* **17**, 118–132 (1990).
23. A. D'Amico-Martel, D. M. Noden, Contributions of placodal and neural crest cells to avian cranial peripheral ganglia. *Am. J. Anat.* **166**, 445–468 (1983).
24. V. M. Lee, J. W. Sechrist, S. Luetolf, M. Bronner-Fraser, Both neural crest and placode contribute to the ciliary ganglion and oculomotor nerve. *Dev. Biol.* **263**, 176–190 (2003).
25. J. A. Ankrum, J. F. Ong, J. M. Karp, Mesenchymal stem cells: Immune evasive, not immune privileged. *Nat. Biotechnol.* **32**, 252–260 (2014).
26. M. Kaucka *et al.*, Analysis of neural crest-derived clones reveals novel aspects of facial development. *Sci. Adv.* **2**, e1600060 (2016).
27. M. J. Carr *et al.*, Mesenchymal precursor cells in adult nerves contribute to mammalian tissue repair and regeneration. *Cell Stem Cell* **24**, 240–256.e9 (2019).
28. M. Kaucka *et al.*, Oriented clonal cell dynamics enables accurate growth and shaping of vertebrate cartilage. *eLife* **6**, e25902 (2017).
29. L. J. Ng *et al.*, SOX9 binds DNA, activates transcription, and coexpresses with type II collagen during chondrogenesis in the mouse. *Dev. Biol.* **183**, 108–121 (1997).
30. Q. Zhao, H. Eberspaecher, V. Lefebvre, B. De Crombrugghe, Parallel expression of Sox9 and Col2a1 in cells undergoing chondrogenesis. *Dev. Dyn.* **209**, 377–386 (1997).
31. I. Adameyko, F. Lallemend, Glial versus melanocyte cell fate choice: Schwann cell precursors as a cellular origin of melanocytes. *Cell. Mol. Life Sci.* **67**, 3037–3055 (2010).
32. L. F. Bonewald, The amazing osteocyte. *J. Bone Miner. Res.* **26**, 229–238 (2011).
33. Y. A. Pan *et al.*, Zebrabow: Multispectral cell labeling for cell tracing and lineage analysis in zebrafish. *Development* **140**, 2835–2846 (2013).
34. A. Kumar, J. W. Godwin, P. B. Gates, A. A. Garza-Garcia, J. P. Brockes, Molecular basis for the nerve dependence of limb regeneration in an adult vertebrate. *Science* **318**, 772–777 (2007).
35. I. Brownell, E. Guevara, C. B. Bai, C. A. Loomis, A. L. Joyner, Nerve-derived sonic hedgehog defines a niche for hair follicle stem cells capable of becoming epidermal stem cells. *Cell Stem Cell* **8**, 552–565 (2011).
36. W. Li *et al.*, Peripheral nerve-derived CXCL12 and VEGF-A regulate the patterning of arterial vessel branching in developing limb skin. *Dev. Cell* **24**, 359–371 (2013).
37. A. Achilleos, P. A. Trainor, Neural crest stem cells: Discovery, properties and potential for therapy. *Cell Res.* **22**, 288–304 (2012).
38. M. Gajda *et al.*, Development of rat tibia innervation: Colocalization of autonomic nerve fiber markers with growth-associated protein 43. *Cells Tissues Organs* **191**, 489–499 (2010).
39. S. A. Green, B. R. Uy, M. E. Bronner, Ancient evolutionary origin of vertebrate enteric neurons from trunk-derived neural crest. *Nature* **544**, 88–91 (2017).
40. M. E. Kastriti, I. Adameyko, Specification, plasticity and evolutionary origin of peripheral glial cells. *Curr. Opin. Neurobiol.* **47**, 196–202 (2017).
41. K. Nakashima *et al.*, The novel zinc finger-containing transcription factor osterix is required for osteoblast differentiation and bone formation. *Cell* **108**, 17–29 (2002).
42. C. Maes, Signaling pathways effecting crosstalk between cartilage and adjacent tissues: Seminars in cell and developmental biology: The biology and pathology of cartilage. *Semin. Cell Dev. Biol.* **62**, 16–33 (2017).
43. C. Maes *et al.*, Osteoblast precursors, but not mature osteoblasts, move into developing and fractured bones along with invading blood vessels. *Dev. Cell* **19**, 329–344 (2010).
44. T. Matsuoka *et al.*, Neural crest origins of the neck and shoulder. *Nature* **436**, 347–355 (2005).
45. J. Isern *et al.*, The neural crest is a source of mesenchymal stem cells with specialized hematopoietic stem cell niche function. *eLife* **3**, e03696 (2014).
46. K. S. Joeng *et al.*, Osteocyte-specific WNT1 regulates osteoblast function during bone homeostasis. *J. Clin. Invest.* **127**, 2678–2688 (2017).
47. C. M. Laine *et al.*, WNT1 mutations in early-onset osteoporosis and osteogenesis imperfecta. *N. Engl. J. Med.* **368**, 1809–1816 (2013).
48. J. Luther *et al.*, Wnt1 is an Lrp5-independent bone-anabolic Wnt ligand. *Sci. Transl. Med.* **10**, eaau7137 (2018).
49. M. M. Weivoda *et al.*, Osteoclast TGF-β receptor signaling induces Wnt1 secretion and couples bone resorption to Bone Formation. *J. Bone Miner. Res.* **31**, 76–85 (2016).
50. S. F. Gilbert, M. J. F. Barresi, *Developmental Biology* (Sinauer Associates, Sunderland, MA, ed. 11, 2016).
51. P. T. Newton, M. Xie, E. V. Medvedeva, L. Sävendahl, A. S. Chagin, Activation of mTORC1 in chondrocytes does not affect proliferation or differentiation, but causes the resting zone of the growth plate to become disordered. *Bone Rep.* **8**, 64–71 (2018).
52. F. Müller, H. Rohrer, Molecular control of ciliary neuron development: BMPs and downstream transcriptional control in the parasympathetic lineage. *Development* **129**, 5707–5717 (2002).
53. C. Laranjeira *et al.*, Glial cells in the mouse enteric nervous system can undergo neurogenesis in response to injury. *J. Clin. Invest.* **121**, 3412–3424 (2011).
54. A. Mongera *et al.*, Genetic lineage labeling in zebrafish uncovers novel neural crest contributions to the head, including gill pillar cells. *Development* **140**, 916–925 (2013).
55. R. E. Mitchell *et al.*, New tools for studying osteoarthritis genetics in zebrafish. *Osteoarthritis Cartilage* **21**, 269–278 (2013).

DEVELOPMENTAL BIOLOGY